Advances in Applied Mathematics and Mechanics
Adv. Appl. Math. Mech., Vol. **6**, No. 6, pp. 764-782

DOI: 10.4208/aamm.2014.m533
December 2014

A Modeling Study on Particle Dispersion in Wall-Bounded Turbulent Flows

Jian-Hung Lin and Keh-Chin Chang*

Department of Aeronautics and Astronautics, National Cheng Kung University, No. 1, University Rd, Tainan 701, Taiwan

Received 10 March 2014; Accepted (in revised version) 23 May 2014

Available online 7 August 2014

Abstract. Three physical mechanisms which may affect dispersion of particle's motion in wall-bounded turbulent flows, including the effects of turbulence, wall roughness in particle-wall collisions, and inter-particle collisions, are numerically investigated in this study. Parametric studies with different wall roughness extents and with different mass loading ratios of particles are performed in fully developed channel flows with the Eulerian-Lagrangian approach. A low-Reynolds-number $k-\epsilon$ turbulence model is applied for the solution of the carrier-flow field, while the deterministic Lagrangian method together with binary-collision hard-sphere model is applied for the solution of particle motion. It is shown that the mechanism of inter-particle collisions should be taken into account in the modeling except for the flows laden with sufficiently low mass loading ratios of particles. Influences of wall roughness on particle dispersion due to particle-wall collisions are found to be considerable in the bounded particle-laden flow. Since the investigated particles are associated with large Stokes numbers, i.e., larger than $\mathcal{O}(1)$, in the test problem, the effects of turbulence on particle dispersion are much less considerable, as expected, in comparison with another two physical mechanisms investigated in the study.

AMS subject classifications: 65M10, 78A48

Key words: Particle-laden flow, turbulent dispersion, inter-particle collision, particle-wall collision.

1 Introduction

Understanding the physical mechanisms which affect particle motion in turbulent flow is a prerequisite for accurate predictions of turbulent quantities of particles. For instances, it is well agreed that the effect of turbulence on particle, i.e., turbulent dispersion, has

*Corresponding author.
Email: kcchang@mail.ncku.edu.tw (K. C. Chang)

to be considered under the condition of Stokes numbers (St) less than $\mathcal{O}(1)$, where the Stokes number is defined as the ratio of the particle relaxation time (τ_p) to the turbulence characteristic time (τ_f). Sommerfeld [1] showed significance of inter-particle collisions in the cases with $\tau_p/\tau_c > \mathcal{O}(1)$, where τ_c denotes the mean free time of particle collisions. Moreover, the experimental study of Benson and Eaton [2] revealed remarkable effects of particle-wall collisions on particle dispersion in the bounded turbulent flows laden with the particles of relatively large St values (i.e., $St > \mathcal{O}(1)$). Particle-wall collision particularly occurred in rough walls have been shown [3, 4] to play a significant role in predictions of particle dispersion in a number of wall-bounded turbulent flows because the particles that collide with a rough wall have a tendency to be suspended into the flow.

In this study, the effects of turbulence, inter-particle collisions, and particle-wall collisions on particle dispersion are numerically investigated by using the Eulerian-Lagrangian approach in fully developed, turbulent flows laden with the particles of various mass loading ratios. Traditional approach based on the Reynolds-averaged Navier-Stokes (RANS) equations together with a low Reynolds number $k-\epsilon$ turbulence model is applied for the solution of the carrier-fluid flow field [5], while the stochastic separated flow model [6] is applied for the solution of the dispersed-phase (i.e., particles) flow field.

2 Test problem

The experimental work on fully developed, turbulent downward channel flow laden with particles at various mass loading ratios conducted by Kulick et al. [7] is chosen as the test problem. Although the investigated problem is a fully developed flow, a three-dimensional flow model is used to account for the 3-dimensional nature of the inter-particle collisions for the translating and rotating particles. The hydraulic diameter of this channel is equal to the half heights (i.e., $D_h = H/2 = 0.02$m). The mean stream-wise velocity of the carrier fluid (air) at the inlet is equal to 10.5m/s, which corresponds to the Reynolds number, based on the hydraulic diameter, of 13,800. The length of this channel ($L_{\text{exp}} = 5.2$m) is sufficiently long ($L_{\text{exp}}/D_h = 260$) to assure both carrier-fluid and particles reaching their fully developed conditions in the downstream of channel. Here, the fully developed condition for particles denotes a phenomenon that the particle motion has reached its own terminal velocity. The ratio of the width of this channel ($W_{\text{exp}} = 0.457$m) to D_h is 23. The span-wise wall effects can be, thus, negligible in the span-wisely central regions. In order to save the computational expenditure, a computational domain in form of Cartesian coordinate is set as 1m(L) $\times$ 0.04m(H) $\times$ 0.01m(W) as schematically shown in Fig. 1 in this study.

3 Physical modeling

The low-Reynolds-number version of the $k-\epsilon$ turbulence model is capable of simulating the fully developed channel flows, including the near-wall regions, which possess some-

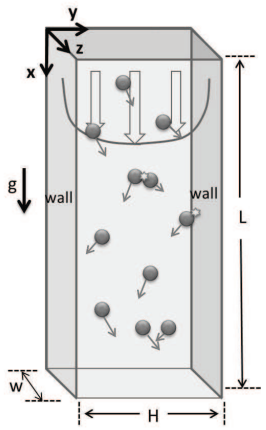

Figure 1: Configuration for the computational domain of the downward vertical channel.

what simple turbulence structure. Since the volumetric fractions occupied by the loading particles are no larger than the order of 10^{-4} in the test problem, the void fraction of the carrier fluid can be reasonably approximated as unity in the modeling. The instantaneous velocity of either carrier-fluid or particle for i^{th} direction which is denoted in upper case (U_i) is decomposed into the mean (u_i) and the fluctuating (u'_i) components in this study.

3.1 Governing equations of carrier fluid

The Reynolds-averaged governing equations coupled with the low Reynolds number $k-\epsilon$ turbulence model developed by Abe et al. [5] for incompressible flow are given below.

Continuity:

$$\frac{\partial u_{g_i}}{\partial x_i}=0. \tag{3.1}$$

Momentum:

$$\frac{\partial(\rho_g u_{g_i})}{\partial t}+\frac{\partial}{\partial x_j}(\rho_g u_{g_j}u_{g_i})=-\frac{\partial p}{\partial x_j}+\frac{\partial}{\partial x_j}\left[(\mu+\mu_t)\left(\frac{\partial u_i}{\partial x_j}+\frac{\partial u_j}{\partial x_i}-\frac{2}{3}\delta_{ij}k\right)\right]+\rho_g g_i+S_{pu_i}. \tag{3.2}$$

Turbulence kinetic energy:

$$\frac{\partial(\rho_g k)}{\partial t}+\frac{\partial}{\partial x_j}(\rho_g u_{g_j}k)=\frac{\partial}{\partial x_j}\left[\left(\mu+\frac{\mu_t}{\sigma_k}\right)\frac{\partial k}{\partial x_j}\right]+P_k-\rho_g\epsilon-S_{pk}. \tag{3.3}$$

Dissipation rate of turbulence kinetic energy:

$$\frac{\partial(\rho_g \epsilon)}{\partial t}+\frac{\partial}{\partial x_j}(\rho_g u_{g_j}\epsilon)=\frac{\partial}{\partial x_j}\left[\left(\mu+\frac{\mu_t}{\sigma_\epsilon}\right)\frac{\partial \epsilon}{\partial x_j}\right]+C_{\epsilon 1}\frac{\rho_g\epsilon}{k}P_k-C_{\epsilon 2}f_\epsilon\frac{\rho_g\epsilon^2}{k}-S_{p\epsilon}, \tag{3.4}$$

where the eddy viscosity, μ_t, and the turbulence production term, P_k, are given, respectively, by

$$\mu_t = C_\mu f_\mu \rho_g \frac{k^2}{\epsilon}, \tag{3.5a}$$

$$P_k = \mu_t \Big(\frac{\partial u_{g_i}}{\partial x_j} + \frac{\partial u_{g_j}}{\partial x_i} \Big) \frac{\partial u_{g_i}}{\partial x_j}. \tag{3.5b}$$

Here f_ϵ and f_μ, which are appeared in Eqs. (3.4) and (3.5a), respectively, are two damping functions accounting for the viscous effects in the near-wall flow region and are given by

$$f_\epsilon = \Big[1-\exp\Big(-\frac{y^+}{3.1}\Big)\Big]^2 \Big\{1-0.3\exp\Big[-\Big(\frac{Re_t}{6.5}\Big)^2\Big]\Big\}, \tag{3.6a}$$

$$f_\mu = \Big[1-\exp\Big(-\frac{y^+}{14}\Big)\Big]^2 \Big\{1+\frac{5.0}{{Re_t}^{3/4}}\exp\Big[-\Big(\frac{Re_t}{200}\Big)^2\Big]\Big\}, \tag{3.6b}$$

where

$$y^+ = \frac{y u_\tau}{\nu}, \tag{3.7a}$$

$$u_\tau = \sqrt{\frac{\tau_w}{\rho}}, \tag{3.7b}$$

$$Re_t = \frac{k^2}{\nu\epsilon}. \tag{3.7c}$$

The values of the empirical constants of $C_{\epsilon 1}$, $C_{\epsilon 2}$, C_μ, σ_k and σ_ϵ appeared in Eqs. (3.3)-(3.5a) are summarized in Table 1.

Table 1: Values of the empirical constants used in the low-Reynolds-number $k-\epsilon$ model.

$C_{\epsilon 1}$	$C_{\epsilon 2}$	C_μ	σ_k	σ_ϵ
1.5	1.9	0.09	1.4	1.4

3.2 Source terms in carrier fluid due to fluid-particle interactions

The S_{pu_i} term shown in Eq. (3.2) represents the momentum exchange rate between the carrier fluid and particles and is calculated using the PSI-cell method [8] in a specified grid cell as

$$S_{p_{u_i}} = \sum_{l=1}^{N} m_p^l [(U_{p_i}^l)_{in} - (U_{p_i}^l)_{out}]/\Delta V, \tag{3.8}$$

where N is the total number of particles passing through the specified cell within a given time step Δt, and ΔV is the volume of the specified cell. To account for the effects of turbulence modulation, two fluid-particle interaction terms S_{p_k} and S_{p_ϵ} are introduced in

Eqs. (3.3) and (3.4) as the additional source terms, respectively, and are modeled as the ones suggested by Lightstone et al. [9]:

$$S_{p_k}=\frac{2k\theta_p}{\tau_p}\Big(1-\frac{\tau^*}{\tau^*+\tau_p}\Big), \tag{3.9a}$$

$$S_{p_\epsilon}=\frac{2\epsilon\theta_p}{\tau_p}\Big(1-\frac{\tau^*}{\tau^*+\tau_p}\Big), \tag{3.9b}$$

where

$$\tau^*=\Big(\frac{\epsilon}{0.135k}+\frac{\epsilon\cdot|\mathbf{u_p}-\mathbf{u_g}|}{0.22k^{1.5}}\Big)^{-1}, \tag{3.10a}$$

$$\tau_p=\frac{\rho_p d_p^2}{18\mu_g}, \tag{3.10b}$$

$$\theta_p=\sum_{l=1}^{N}\frac{m_p^l}{\Delta V}. \tag{3.10c}$$

3.3 Equations of particle motion

Equations of particle motion consist of translation and rotation parts, which are expressed, respectively, as follows.

Translation:

$$m_p\frac{d\mathbf{U_p}}{dt}=\mathbf{F_D}+\mathbf{F_S}+\mathbf{F_M}+\mathbf{F_G}. \tag{3.11}$$

Rotation:

$$I_p\frac{d\mathbf{\Omega_p}}{dt}=\mathbf{T_V}. \tag{3.12}$$

Note that the virtual mass, Basset history and buoyancy forces have been neglected due to a fact that the density ratios between particles and carrier fluid are equal to $\mathcal{O}(10^3)$ in the test problem. The quasi-steady drag force $\mathbf{F_D}$ is determined by the empirical drag coefficient C_D in terms of the particle Reynolds number, Re_p, which is suggested by Schiller and Naumann [10] as

$$\mathbf{F_D}=\frac{\pi}{8}\rho_g C_d d_p^2|\mathbf{U_g}-\mathbf{U_p}|(\mathbf{U_g}-\mathbf{U_p}), \tag{3.13}$$

where

$$C_D=\frac{24}{Re_p}(1+0.15Re_p^{0.687}), \tag{3.14a}$$

$$Re_p=\frac{\rho_g d_p|\mathbf{U_g}-\mathbf{U_p}|}{\mu}. \tag{3.14b}$$

The Saffman lift force $\mathbf{F_S}$ is due to the velocity gradient of the carried fluid surrounding a particle. It is determined using the fitted expression of Mei et al. [11] as

$$\mathbf{F_s} = 1.61 \cdot f_s \cdot d_p^2 (\rho_g \mu)^{\frac{1}{2}} |\mathbf{\Omega_g}|^{-\frac{1}{2}} [(\mathbf{U_g} - \mathbf{U_p}) \times \mathbf{\Omega_g}], \tag{3.15}$$

where $\mathbf{\Omega_g}$ is the carrier-fluid vorticity vector defined by

$$\mathbf{\Omega_g} = \bigtriangledown \times \mathbf{U_g} \tag{3.16}$$

and

$$f_s = \begin{cases} (1 - 0.3314\beta^{\frac{1}{2}}) \exp\left(-\dfrac{Re_p}{10}\right) + 0.3314\beta^{\frac{1}{2}}, & \text{for } Re_p \leq 40, \\ 0.0524(\beta Re_p)^{\frac{1}{2}}, & \text{for } Re_p > 40, \end{cases} \tag{3.17a}$$

$$\beta = \frac{d_p}{2|\mathbf{U_g} - \mathbf{U_p}|} |\mathbf{\Omega_g}|. \tag{3.17b}$$

The Magnus lift force $\mathbf{F_M}$ accounts for the effect of particle's rotation and is determined using the empirical lift coefficient in term of Re_p and Re_r as suggested by Oesterle and Bui Dinh [12]:

$$\mathbf{F_M} = \frac{\pi}{8} \rho_g |\mathbf{U_g} - \mathbf{U_p}| C_{LR} d_p^2 \Big[\frac{(\mathbf{U_g} - \mathbf{U_p}) \times (\mathbf{\Omega_p} - \mathbf{0.5\Omega_g})}{(\mathbf{\Omega_p} - \mathbf{0.5\Omega_g})} \Big], \tag{3.18}$$

where

$$C_{LR} = 0.45 + \left(\frac{Re_p}{Re_r} - 0.45\right) \exp(-0.05684 Re_r^{0.4} Re_p^{0.3}), \tag{3.19a}$$

$$Re_r \equiv \frac{\rho_g d_p |\mathbf{\Omega_p} - \mathbf{0.5\Omega_g}|}{4\mu}. \tag{3.19b}$$

The momentum inertia I_p shown in Eq. (3.12) is defined by

$$I_p = \frac{1}{10} m_p d_p^2. \tag{3.20}$$

The viscous torque is induced by the viscous shear force on the rotating particle and is determined by [13, 14]

$$\mathbf{T_V} = -C_{T_v} \frac{\rho_g}{2} \left(\frac{d_p}{2}\right)^5 |\mathbf{\Omega_p} - \mathbf{0.5\Omega_g}| (\mathbf{\Omega_p} - \mathbf{0.5\Omega_g}), \tag{3.21}$$

where the coefficient C_{T_v} is a function of Re_τ and is expressed by

$$C_{T_v} = C_{\tau_1} \cdot Re_r^{-0.5} + C_{\tau_2} \cdot Re_r^{-1.5} + C_{\tau_3} \cdot Re_r. \tag{3.22}$$

The values of C_{τ_1}, C_{τ_2} and C_{τ_3} in various ranges of Re_r are listed in Table 2.

Table 2: Values of C_{τ_1}, C_{τ_2} and C_{τ_3} in various Re_r ranges [15].

Re_r range	C_{τ_1}	C_{τ_2}	C_{τ_3}
$Re_r \leq 1$	0.0	16π	0.0
$1 < Re_r \leq 10$	0.0	16π	0.0418
$10 < Re_r \leq 20$	5.32	37.2	0.0
$20 < Re_r \leq 50$	6.44	37.2	0.0
$50 < Re_r$	6.45	32.1	0.0

3.4 Inter-particles collisions

Searching for inter-particle collisions is deterministically made with uncoupling technique of binary-collision hard-sphere model [16]. There are two steps in searching for the particle collision pair. First, all particles are advanced to the next time step $(t+\Delta t)$ through solving the equations of motion without taking into account inter-particle collisions as shown in Fig. 2. Second, particle collision pair is conditioned by the following relationship

$$|\mathbf{r_t}+\lambda(\mathbf{r_{t+\Delta t}}-\mathbf{r_t})|^2=\frac{(d_i+d_j)^2}{4}, \tag{3.23}$$

which states the distance between two particles (say the particles i and j as shown in Fig. 2 equal to the sum of their radii, i.e., $(d_i/2+d_j/2)$, during Δt. This relationship yields a quadratic equation for λ. If there exist two real roots, λ_1 and λ_2, $(\lambda_1 \leq \lambda_2)$, in the resultant quadratic equation and $0<\lambda_1 \leq 1$, a collision takes place between these two particles at the time $t+\lambda\Delta t$, as schematically shown in Fig. 2.

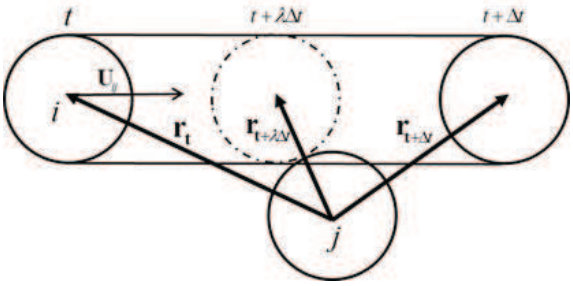

Figure 2: Schematics for searching collision pair in binary collision process.

When a collision is identified, the post-collision velocities for the collision pair are updated in accordance with the inelastic hard-sphere model as

$$\mathbf{U}^*_{\mathbf{p_i}}=\mathbf{U}_{\mathbf{p_i}}+\frac{\mathbf{J}}{m_p}, \tag{3.24a}$$

$$\mathbf{U}^*_{\mathbf{p_j}} = \mathbf{U}_{\mathbf{p_j}} - \frac{\mathbf{J}}{m_p}, \tag{3.24b}$$

$$\mathbf{\Omega}^*_{\mathbf{p_i}} = \mathbf{\Omega}_{\mathbf{p_i}} + \frac{d_i}{2I_p}\mathbf{e_n} \times \mathbf{J}, \tag{3.24c}$$

$$\mathbf{\Omega}^*_{\mathbf{p_j}} = \mathbf{\Omega}_{\mathbf{p_j}} - \frac{d_i}{2I_p}\mathbf{e_n} \times \mathbf{J}. \tag{3.24d}$$

Here the impulse force vector $\mathbf{J}$ is composed of the tangential (J_t) and normal (J_n) components which are expressed in [17], respectively, by

$$J_t = \begin{cases} -\frac{2}{7}\frac{m_{pi}m_{pj}}{m_{pi}+m_{pj}}|(\mathbf{U_{ct}})_{\mathbf{ij}}|, & \text{for } J_t < f \cdot J_n, \\ -fJ_n, & \text{for } J_t > f \cdot J_n, \end{cases} \tag{3.25a}$$

$$J_n = -\frac{m_{pi}m_{pj}}{m_{pi}+m_{pj}}(1+e)(\mathbf{U_{ij}} \cdot \mathbf{e_n}), \tag{3.25b}$$

where e and f are the normal restitution coefficient and frictional coefficient of the particle, respectively, and are given with the values of 0.995 and 0.3, respectively, in the present study; $(\mathbf{U_{ij}})$ is the relative velocity vector of the particle i to the particle j at the contact point during collision and can be expressed as

$$(\mathbf{U_{ct}})_{ij} = \mathbf{U_{p_i}} - \mathbf{U_{p_j}} + \frac{d_i}{2}\mathbf{\Omega_{p_i}} \times \mathbf{e_n} + \frac{d_j}{2}\mathbf{\Omega_{p_j}} \times \mathbf{e_n}. \tag{3.26}$$

Here $\mathbf{e_n}$ and $\mathbf{e_t}$ represent the unit vectors along normal and tangential directions, respectively, at the contact point of two particles i and j during collision, and are given by

$$\mathbf{e_n} = -\frac{\mathbf{r}_{t+\lambda_1\Delta t}}{|\mathbf{r}_{t+\lambda_1\Delta t}|}, \tag{3.27a}$$

$$\mathbf{e_t} = -\frac{(\mathbf{U_{ct}})_{\mathbf{ij}}}{|(\mathbf{U_{ct}})_{\mathbf{ij}}|}. \tag{3.27b}$$

The post-collision positions of the collision pair are updated by the corresponding values of $[\mathbf{r}_{t+\lambda_1\Delta t} + (1-\lambda_1)\Delta t \cdot \mathbf{U}^*]$. Since determination of the computational time step follows the criteria of $\Delta t/\tau_c \leq \mathcal{O}(10^{-3})$, it can be reasonably assumed that there is no secondary collision for the particle i in a given Δt. Hence, no further search for the collision pair is performed in the remaining time step, i.e., $(1-\lambda_1)\Delta t$, for the particle i.

3.5 Particle-wall collisions

An estimated particle size, for which particle-wall collisions dominate the particle motion in a fully developed channel flow, was suggested by Sommerfeld [18] as

$$d_p > \sqrt{\frac{18\mu H}{0.7\rho_p \overline{(v'_p)_{rms}}}}, \tag{3.28}$$

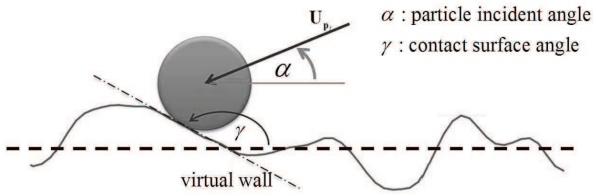

Figure 3: Illustration of particle collision on a rough-wall surface.

where $\overline{(v_p')_{rms}}$ is the sectionally averaged root-mean-squared (rms) transverse (wall-normal) velocity fluctuation. Sommerfeld further assumed that

$$\overline{(v_p')_{rms}} = K\overline{u_p}, \tag{3.29}$$

where $\overline{u_p}$ is sectionally averaged axial particle mean velocity. As applied to the data reported in the experiments of Kulick et al. [7], the K values were estimated in the range between $0.015-0.025$. Based on Eq. 3.28 together with Eq. (3.29), the diameter, defining a wall-collision-dominated two-phase flow, falls within $38-50\mu m$ for copper particles, which will be smaller than the sizes of copper particles (70 and $90\mu m$) used in the experiments of Kulick et al. [7]. In other words, the particle-wall collisions in rough walls have to be considered in the present modeling.

Since the wall roughness may be changed with time due to constant occurrence of particle-wall collisions, a stochastic model for virtual rough wall (illustrated in Fig. 3) developed by Sommerfeld and Huber [19] is adopted in this study. The probability distribution function of contact surface angle (γ), P_{col}, at a given incident angle of particle (α) and a standard deviation of γ, $\Delta\gamma$, is expressed as

$$P_{col}(\alpha,\Delta\gamma,\gamma) = \max\Big\{0, \frac{1}{\sqrt{2\pi}\Delta\gamma}\exp\Big[-\frac{1}{2}\Big(\frac{\gamma}{\Delta\gamma}\Big)^2\Big]\frac{\sin(\alpha+\gamma)}{\sin(\alpha)}\Big\}. \tag{3.30}$$

Details of the sampling algorithm for this virtual wall approach is referred to [19].

3.6 Particle dispersion due to turbulence

Solution of the equations of instantaneous particle motion, i.e., Eqs. (3.11) and (3.12) reguire the input of the instantaneous velocity of the carrier fluid. Nevertheless, only the mean quantities of the carrier-fluid velocity components are provided in the solutions of the RANS governing equations. The fluctuating velocity of carrier fluid along the particle trajectory is generated using the Langevin method [20] as follows.

$$(u_{g_i}')_{t+\Delta t} = (u_{g_i}')_t\, R + G_i[(u_{gi}')_t](u_{gi}')_{rms}\sqrt{1-R^2}, \tag{3.31}$$

where $G_i[(u_{gi}')_t]$ is the normalized Gaussian distribution function with zero mean and unit variance for i^{th} velocity component, and R is the autocorrelation function expressed

by [21–23]

$$R=\exp(-\Delta t/T_L). \tag{3.32}$$

Here the Lagrangian integral time scale T_L is estimated by

$$T_L=\frac{2}{C_0}\frac{k}{\epsilon}. \tag{3.33}$$

The first term on the right hand side in Eq. (3.31) represents the correlated part, while the second term contributes the random fluctuation of turbulence.

4 Numerical aspects and boundary conditions

The carrier-fluid governing equations are solved with the commercial code, ANSYS FLUENT (Version 13.0.0) [24], which uses the finite volume method incorporated with the third-order QUICK scheme [25] and SIMPLE algorithm [26] as the solver. A non-uniform grid mesh with in x-, y- and z-directions, which assures nearly grid independent solution of the carrier-fluid, is applied. To ensure the employed low-Reynolds number $k-\epsilon$ model [5] working normally, the dimensionless position values of the first nodes away from the channel wall, ${y_p}^+$, are around unity. The equations of particle motion for both translation and rotation are solved by iteratively integrating the non-linear first-order differential equations to an acceptable tolerance in a specified Δt. The fully developed profiles of all dependent variables for the carrier-fluid, except for the mean span-wise velocity (w_g), in the flow case without loading particles investigated in the experiments of Kulick et al. [7] are initially assigned as the inlet conditions. The initial inlet profile of w_g is assumed to be same as the one of mean transverse velocity (v_g). Distribution of u_{p_i} at the inlet are initially set as same as that of u_{g_i}. Outlet conditions for all dependent variables of the carrier fluid are set equal to zero derivatives. Due to the fully developed conditions of the test problem, the outlet profiles for both carrier fluid and particles obtained in a complete computational procedure are re-assigned as the updated inlet conditions. The computational procedure is repeated until the differences between all the velocity components of the carrier fluid and particles at the inlet and those corresponding ones at the outlet are converged within 1%. (each normalized with the sectionally averaged axial mean value of u_g at the inlet, i.e., $\overline{u_g}$, which is given in the experiment). No-slip condition for carrier-fluid velocity is used.

5 Results and discussion

The effects of turbulence, wall roughness in particle-wall collisions, and inter-particle collisions on the predictions of turbulence quantities of particles are parametrically studied with the test problem laden with $70\mu m$ copper particles [7] under various mass loading ratios ranging from 2 to 40%. All the results presented hereafter are subject to the fully developed conditions.

5.1 Effects of turbulence on particle dispersion

Different C_0 values appeared in Eq. (3.33) were reported in the literatures. For examples, Du et al. [21] and Sawford [22] concluded $C_0 = 3.0 \pm 0.5$ and 7.0, respectively, from their simulation in grid turbulence, while Mito and Hanratty [23] suggested $C_0 = 14.0$ since it led to a satisfactory agreement with the direct numerical simulation (DNS) data in a channel flow. Thus, these three C_0 values are tested with 2% mass loading ratio. Note that only axial and transverse components of mean and rms fluctuating velocities for both carrier fluid and particles were measured in the experiments of Kulick et al. [7], and not all measured data were presented in their paper. The sectional profiles of normalized u_p, $(u'_p)_{rms}$ and $(v'_p)_{rms}$ predicted with three C_0 values are presented in Fig. 4. Since the flow is symmetric with respect to $y = H/2$ along transverse direction, the results are presented in half of the domain only ($0.5H$, see Fig. 1) in Fig. 4 and all the following figures in this study. Effects of C_0 value on u_p and $(v'_p)_{rms}$ are insignificant, while on $(u'_p)_{rms}$ is not as considerable as for the other two factors, i.e., wall roughness in particle-wall collisions (Fig. 6b) and inter-particle collisions (Fig. 7b) which will be elaborated later. The Stokes number defined by

$$St = \frac{\tau_p}{\tau_f} = \frac{\rho_p {d_p}^2}{18\mu} \Big/ \frac{k}{\epsilon} \tag{5.1}$$

is calculated for the case with $C_0 = 7.0$ and its sectional distribution is plotted in Fig. 5 to help explain the results appeared in Fig. 4. It shows that St values vary from $\mathcal{O}(10^2)$ in the

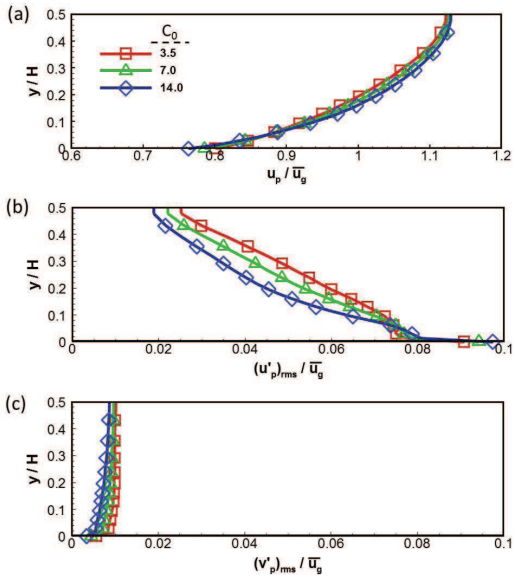

Figure 4: Fully developed distributions of (a) u_p, (b) $(u'_p)_{rms}$ and (c) $(v'_p)_{rms}$ obtained with three different C_0 values in the case with the mass loading ratio of 2%, and wall roughness of $\Delta\gamma = 0.01$.

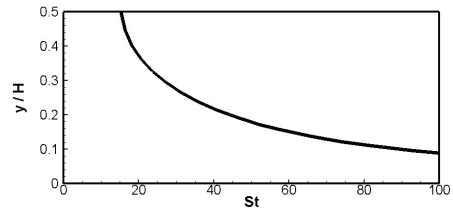

Figure 5: Distribution of Stokes number defined by Eq. (5.1) for the case of $C_0=7.0$ in Fig. 4.

near wall region to $\mathcal{O}(10^1)$ in the central flow region, while are all greater than $\mathcal{O}(10^0)$. This implies that the effects of turbulence on particle dispersion would not be considerable as reported in the results of Fig. 4. Since the choice of C_0 would not considerably affect the turbulent dispersion predictions of particles, the C_0 value is set equal to 7.0 (the mid value among the three tested C_0 values) hereafter in the following calculations.

5.2 Effects of wall roughness extent on particle dispersion

The wall roughness is dependent on the wall material and its surface finish. For example, the typical values of $\Delta\gamma$ for glass, acrylic (PMMA), carbon steel (unpolished), and copper (unpolished) are about 0.0004, 0.008, 0.02 and 0.04, respectively. Six different wall roughness extents ranging from $\Delta\gamma=0$ (smooth wall) to $\Delta\gamma=0.04$ are tested in the cases with 2% mass loading ratio. The predicted profiles of normalized u_p, $(u'_p)_{rms}$ and $(v'_p)_{rms}$ with six different values of $\Delta\gamma$ are presented in Fig. 6. It is seen that the choice of $\Delta\gamma$ in the simulation does affect the predicted results of u_p, $(u'_p)_{rms}$ and $(v'_p)_{rms}$ considerably as shown in Fig. 6. It was reported in the experimental study of Kussin and Sommerfeld [3] that the wall roughness remarkably enhanced the transverse dispersion of particles and their fluctuating velocities throughout the channel. Our predictions on $(v'_p)_{rms}$ (Fig. 6c) are consistent with what they observed. Due to this enhanced transverse transport of particles' momenta, the transverse distributions of u_p and $(u'_p)_{rms}$ become more flattened along with the increased $\Delta\gamma$ as revealed in Figs. 6b and c, respectively. The effects of rough wall has to be, thus, considered in modeling the wall-bounded turbulent flow laden with particles.

5.3 Effects of inter-particles collisions on particle dispersion

Four different mass loading ratios of copper particles, which were studied in the experiments of Kulick et al. [7], including 2, 10, 20 and 40% are tested with $\Delta\gamma$ being set equal to 0.02. Two simulations, each with or without considering the inter-particle collisions in the modeling, are separately performed for these four ratios of mass loading. Comparisons of predicted u_p, $(u'_p)_{rms}$ and $(v'_p)_{rms}$ between the computations with and without considering the inter-particle collisions in the modeling for these four tested mass loading ratios are presented in Fig. 7. The comparisons made between the two computations obtained respectively with and without considering inter-particle collisions for each case

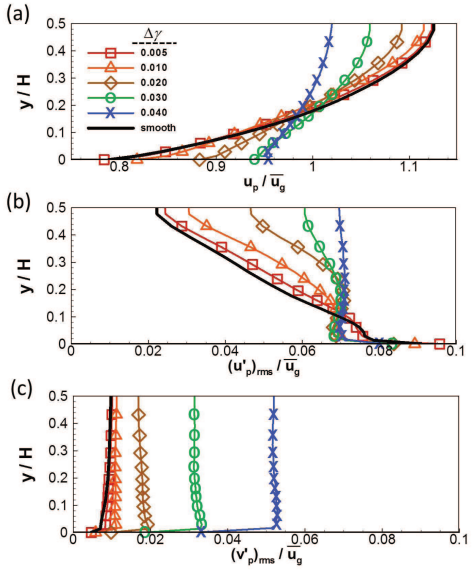

Figure 6: Fully developed distributions of (a) u_p, (b) $(u_p')_{rms}$ and (c) $(v_p')_{rms}$ obtained with six different wall roughness extents in the case with the mass loading ratio of 2%.

reveal a fact that the influences of the inter-particle collisions become gradually considerable along with the increase of mass loading ratio of particles. Thus, the usual neglect of the inter-particle collisions in modeling turbulent particle-laden flow works only for the very dilute case, that is, 2% mass loading ratio of $70\mu m$ copper particles, in the present test problem.

5.4 Comparison of the model predictions with the experimental data [7]

It is noted that there exist relatively complete database in the case of 20% mass loading ratio among all the experimental results reported in the paper [7] for the flow laden with $70\mu m$ copper particles. This case was, thus, selected as the test case for the comparison with model performance. As mentioned before, the inter-particle collisions and the wall roughness extent in particle-wall collisions are two noticeable factors which are capable of affecting the model performance of turbulent particle dispersion. The first simulation is performed by taking into account of these two factors. However, for lack of the wall roughness information in the experimental study of Kulick et al. [7], computations are made with six different values of $\Delta\gamma$ studied in Fig. 6, and each predicted results are individually compared with the available experimental data [7]. It is found that the predicted results of u_p, $(u_p')_{rms}$ and $(v_p')_{rms}$ with $\Delta\gamma = 0.02$ yield the best fit with the experimental data. Thus, this case is selected as one comparison case and named Case 1. Another comparison case is designed with a rough condition of without considering inter-particle collisions and with smooth wall ($\Delta\gamma = 0$), and is termed as Case 2.

The fully-developed distributions of u_g and k, predicted from Cases 1 and 2, are p-

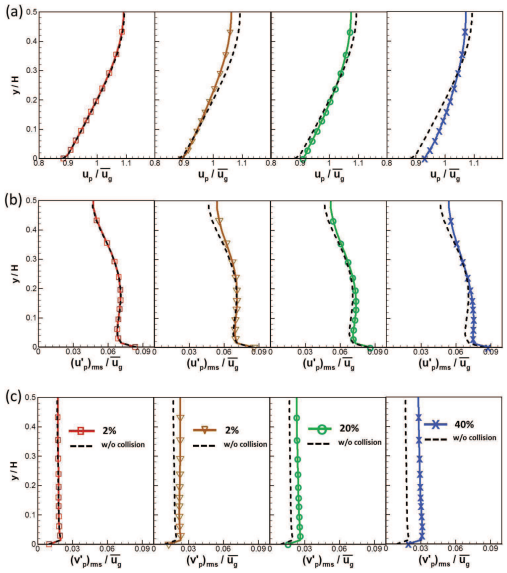

Figure 7: Comparison between two sets of fully developed distributions of (a) u_p, (b) $(u'_p)_{rms}$ and (c) $(v'_p)_{rms}$ obtained with and without considering inter-particle collisions in the case with wall roughness of $\Delta\gamma=0.02$ for the four different mass loading ratios.

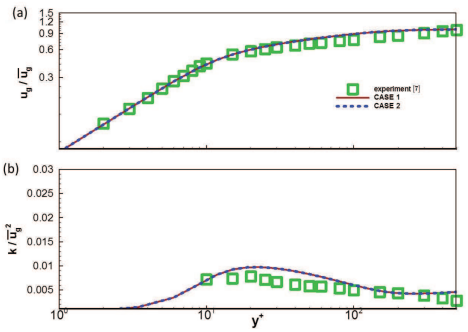

Figure 8: Comparison of two sets of (a) u_g and (b) k obtained with Case 1 (considering inter-particle collisions and wall roughness of $\Delta\gamma=0.02$) and Case 2 (considering no inter-particle collisions and smooth wall) as well as the experimental data [7].

resented in Fig. 8 and compared with the measured data [7]. As noted before, the experimental work of Kulick et al. [7] did not provide the span-wise velocity data for both carrier fluid and particles. However, the calculation of k (turbulence kinetic energy of carrier fluid, which is defined as

$$k=\frac{1}{2}\left[(u'_p)^2_{rms}+(v'_p)^2_{rms}+(w'_p)^2_{rms}\right]$$

reguires the data of the span-wise component, $(w'_p)_{rms}$. An approximation of $(w'_p)_{rms}=(v'_p)_{rms}$, which is usually acceptable in the fully developed flow condition, is made here.

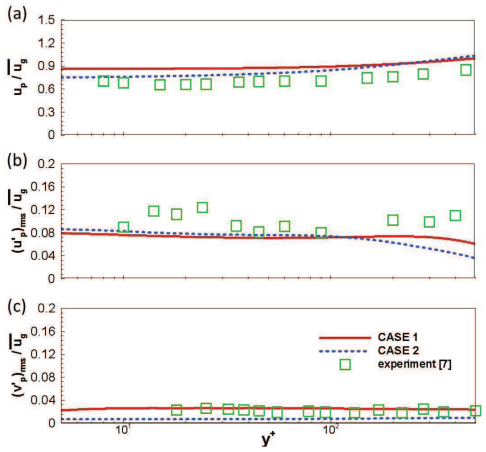

Figure 9: Comparison of the two sets of (a) u_p, (b) $(u'_p)_{rms}$ and $(v'_p)_{rms}$ obtained with Case 1 (considering inter-particle collisions and wall roughness of $\Delta\gamma=0.02$) and Case 2 (considering no inter-particle collisions and smooth wall) as well as the experimental data [7].

Two conclusions can be drawn from the comparisons made from Fig. 8. First is that there are no distinguishable differences between two predictions obtaine/d from Case 1 and Case 2. The second is that the predictions of u_g and k, no matter which case is, are in good agreement with the measured data. It provides an evidence that the employed low-Reynolds-number version of $k-\epsilon$ turbulence model worked well even in the near-wall regions, which, in turn, become a prerequisite for correct prediction of particle dispersion in the near wall regions.

The fully-developed distributions of u_p, $(u'_p)_{rms}$ and $(v'_p)_{rms}$, predicted from Cases 1 and 2, are presented in Fig. 9 and compared with the measured data [7]. The comparison made between the two sets of predictions and the measured data in Fig. 9 shows that the consideration of inter-particle collisions and wall roughness of $\Delta\gamma=0.02$ improves generally the predictions of turbulent particle dispersion. Although the predictions of both u_p and both $(u'_p)_{rms}$ from Cases 1 and 2 are larger and smaller, respectively, than the measu/red data, the slopes of u_p and $(u'_p)_{rms}$ distribution profiles obtained from Case 1 are closer to the measured ones than those from Case 2.

6 Conclusions

A series of parametric studies of the physical mechanisms, including the effects of turbulence, wall roughness in particle-wall collisions, and inter-particle collisions on particle dispersion, are performed in the fully developed channel flows laden with $70\mu m$ copper particles. It is shown that the mechanism of inter-particle collisions should be taken into account in the modeling except for the cases with sufficiently low (2% in the present test problem) mass loading ratios of copper particles. Influences of wall roughness on parti-

cle dispersion due to particle-wall collisions are found to be considerable in the bounded particle-laden flow too. The wall roughness information should be, thus, provided in the experimental study of bounded particle-laden flow in order to attain more accurate predictions of particle dispersion in the consequent numerical simulation. For the particles associated with the large St, i.e., $St > \mathcal{O}(1)$, in the present test problem, the effects of turbulence on particle dispersion are apparently less considerable as compared to the other two mechanisms investigated in the study.

Acknowledgments

This works was done with financial support by National Science Council, R.O.C. under Grant No. NSC 98-2221-E006-132.

Nomenclature

C_D	Drag coefficient, defined by Eq. (3.14a)
C_{LR}	Empirical coefficient of Magnus lift force, defined by Eq. (3.19a)
C_{T_V}	Empirical coefficient of viscous torque, defined by Eq. (3.22)
$C_{\epsilon 1}, C_{\epsilon 2}$	Model constants in ϵ equation
C_μ	Model in eddy-viscosity formulation
$C_{\tau_1}, C_{\tau_2}, C_{\tau_3}$	Empirical coefficients in determination of C_{T_V}
C_0	Empirical coefficients in determination of T_L
D_h	Hydraulic diameter of channel, (m)
d_p	particle diameter, (m)
e	Restitution coefficient of particle
f	Friction coefficient of particle
f_s	Empirical function, defined by Eq. (3.17a)
f_ϵ, f_μ	Damping functinos of the low-Reynold-number $k-\epsilon$ model, defined by Eqs. (3.6a) and (3.6b), respectively
g	Gravity, (m/s^2)
G	Gaussian function with zero mean and unit variance
H	Channel height, (m)
I_p	Momentum inertia of particle, defined by Eq. (3.20), $(kg \cdot m^2)$
J_n, J_t	Normal and tangential components of impulse, respectively, $(kg \cdot m/s)$
k	Turbulence kinetic energy, $(kg \cdot m^2/s^2)$
L	Length of computational domain, (m)
L_{exp}	Channel length, (m)
m_p	Mass of particle, (kg)
N	Number of particles passing through a grid cell
p	Pressure, (N/m^2)
P_{col}	Probability density function of contact surface angle

P_k	Turbulence production term, defined by Eq. (3.5b), $(kg\cdot m^2/s^3)$
R	Correlation function
Re	Reynolds number based on hydraulic diameter
Re_p	Particle Reynolds number, defined by Eq. (3.14b)
Re_r	Rotational Reynolds number, defined by Eq. (3.19b)
Re_t	Reynolds number based on characteristic scale of turbulence, defined by Eq. (3.7c)
S_{pu_i},S_{pk},$S_{p\epsilon}$	Source terms accounting for fluid-particle interactions in u_{g_i}, k and ϵ equations, $(kg/m^2\cdot s^2)$, $(kg/m\cdot s^3)$ and $(kg/m\cdot s^4)$, respectively
St	Stokes number
t	Time (s)
T_L	Lagrangian integral time scale, (s)
u,u',U	Mean, fluctuating and instantaneous velocities, respectively, (m/s)
u_τ	Friction velocity, defined by Eq. (3.7b), (m/s)
W	Width of computational domain, (m)
W_{exp}	Channel width, (m)
x	Coordinate, (m)
y,y^+	Dimensional, (m), and dimensionless wall distances, respectively
α	Particle incident angle, $(radian)$
β	Dimensionless parameter, defined by Eq. (3.17b)
γ	Contact surface angle, $(radian)$
δ_{ij}	Dirac delta function
Δt	Time step, (s)
ΔV	Volume of grid cell, (m^3)
$\Delta\gamma$	Standard deviation of γ, $(radian)$
ϵ	Dissipation rate of turbulence kinetic energy, $(kg\cdot m^2/s^3)$
θ_p	Bulk density of particles, (kg/m^3)
λ	Small real root of Eq. (3.23)
μ,μ_t	Molecular and eddy viscosities, respectively, $(kg/m\cdot s)$
ν	kinematic viscosity, (m^2/s)
σ_k,σ_ϵ	Turbulent Prandtl numbers in k and ϵ equations, respectively
τ	Characteristic time scale, (s)
τ^*	Characteristic turbulence time scale, defined by Eq. (3.10a), (s)
τ_c	Mean free time for inter-particle collisions, (s)
τ_f	Characteristic time of flow field, (s)
τ_p	Particle relaxation time, defined by Eq. (3.10b), (s)
τ_w	Wall shear stress, $(kg/m\cdot s^2)$
ρ_g,ρ_p	Densities of gas and particle, respectively, (kg/m^3)
$\mathbf{e_n}$,$\mathbf{e_t}$	Unit vectors of the directions normal and tangential, respectively, to the collision surface
$\mathbf{F_D}$	Drag force vector, (N)
$\mathbf{F_G}$	Gravitational force vector, (N)

$\mathbf{F_M}$	Magnus lift force vector, (N)
$\mathbf{F_S}$	Saffman lift force vector, (N)
$\mathbf{e_n}$,$\mathbf{e_t}$	Unit vectors of the directions normal and tangential, respectively, to the collision surface
$\mathbf{F_D}$	Drag force vector, (N)
$\mathbf{F_G}$	Gravitational force vector, (N)
$\mathbf{F_M}$	Magnus lift force vector, (N)
$\mathbf{F_S}$	Saffman lift force vector, (N)
$\mathbf{J}$	Impulse between two particles in collision, $(kg\cdot m/s)$
$\mathbf{r}$	Relative position vector between two particles, (m)
$\mathbf{T_V}$	Viscous torque vector of particle, $(N\cdot m)$
$\mathbf{U_{ij}}$	Relative velocity vector between two particles, (m/s)
$\mathbf{U_p}$	Instantaneous velocity vector of particle, (m/s)
$(\mathbf{U_{ct}})_{\mathbf{ij}}$	Relative velocity vector at contact point of two particles, (m/s)
$\mathbf{\Omega_g}$	Carrier-fluid vorticity vector, (s^{-1})
$\mathbf{\Omega_p}$	Angular velocity vector of particle, (s^{-1})
g	Carrier fluid
i,j,k	Stream-wise, wall-normal and span-wise directions, respectively
in,out	Inlet and outlet positions in the grid cell, respectively
p	Particle
rms	Root-mean-squared quantity
t,$t+\Delta t$	At times t and $t+\Delta t$, respectively
$'$	Fluctuating quantity
$*$	Post-collision state
$\bar{}$	Sectionally averaged quantity

References

[1] M. SOMMERFELD, *Analysis of collision effects for turbulent gas-particle flow in a horizontal channel: part I: particles transport*, Int. J. Multiphase Flow, 29 (2003), pp. 675–699.

[2] M. J. BENSON AND J. K. EATON, *The effects of wall roughness on the particle velocity field in fully-developed channel flow*, Report No. TSD-150, Department of Mechanical Engineering, Stanford University, California, 2003.

[3] J. KUSSIN AND M. SOMMERFELD, *Experimental studies on particle behaviour and turbulence modification in horizontal channel flow with different wall roughness*, Exp. Fluids, 33 (2002), pp. 143–159.

[4] M. SOMMERFELD AND J. KUSSIN, *Wall roughness effects on pneumatic conveying of spherical particles in a narrow horizontal channel*, Powder Tech., 142 (2004), pp. 180–192.

[5] K. ABE, T. KONDOH AND Y, NAGANO, *A new turbulence model for predicting fluid flow and heat transfer in separating and reattaching flow I. flow field calculations,* Int. J.Heat Mass Transfer, 37 (1994), pp. 139–151.

[6] C. T. CROWN, T. R. TROUTT AND J. N. CHUNG, *Numerical models for two-phase turbulent flows*, Ann. Rev. Fluid Mech, 28 (1996), pp. 11–43.

[7] J. D. KULICK, J. R. FESSLER, AND J. K. EATON, *Particle response and turbulence modification in fully developed channel flow*, J. Fluid Mech., 277 (1994), pp. 109–134.
[8] C. T. CROWE, M. P. SHARMA AND D. E. STOCK, *The particle-source-in-cell (PSI-cell) model for gas-droplet flows*, Trans. ASME. J. Fluid Eng., 99 (1997), pp. 325–332.
[9] M. F. LIGHTSTONE AND S. M. HODGSON, *Turbulence modulation in gas-particle flows: comparison of selected models*, Can. J. Chem. Eng., 82 (2004), pp. 209–219.
[10] P. R. SCHILLER AND A. NAUMANN, *Uber die grundlegenden berechnungen bei der schwekraftaubereitung*, Zeitschrift des Vereins Deutscher Ingenieure, 77 (1933), pp. 318–320.
[11] R. MEI, *An approximate expression for the shear lift force on a spherical particle at finite Reynolds number*, Int. J. Multiphase Flow, 18 (1992), pp. 145–147.
[12] B. OESTERLE AND T. BUI DINH, *Experiments on the lift of a spinning sphere in a range of intermediate Reynolds numbers*, Exp. Fluids, 25 (1998), pp. 16–22.
[13] S. C. R. DENNIS, S. N. SINGH AND D. B. INGHAM, *The steady flow due to a rotating sphere at low and moderate Reynolds numbers*, J. Fluid Mech., 101 (1980), pp. 257–279.
[14] H. TAKAGI, *Viscous flow induced by slow rotation of a sphere*, J. Phys. Soc. Japan, 42 (1977), pp. 319–325.
[15] Y. PAN, T. TANAKA AND Y. TSUJI, *Turbulence modulation by dispersed solid particles in rotating channel flows*, Int. J. Multiphase Flow, 28 (2002), pp. 527–552.
[16] G. A. BIRD, Molecular Gas Dynamic, Clarendon Press, Oxford, 1976.
[17] T. TANAKA AND M. TSUJI, *Numerical simulation of gas-solid two-phase flow in a vertical pipe: on the effect of inter-particle collision*, in Gas-Solid Flow (FED, Vol. 121, ASME, 1991), pp. 123–128.
[18] M. SOMMERFELD, *Modelling of particle-wall collisions in confined gas-particle flows*, Int. J. Multiphase Flow, 18 (1992), pp. 905–926.
[19] M. SOMMERFELD AND N. HUBER, *Experimental analysis and modelling of particle-wall collisions*, Int. J. Multiphase Flow, 25 (1999), pp. 1457–1489.
[20] F. PASQUILL AND F. B. SMITH, Atmospheric Diffusion 3rd ed., Wiley, New York, 1983.
[21] S. DU, B. L. SAWFORD, J. D. WILSON AND D. J. WILSON, *Estimation of the Kolmogorov constant (C_0) for the Lagrangian structure function, using a second-order Lagrangian model of grid turbulence*, Phys. Fluids, 7 (1995), pp. 3083–3090.
[22] B. L. SAWFORD, *Reynolds number effects in Lagrangian stochastic models of turbulent dispersion*, Phys. Fluids A, 3 (1991), pp. 1577–1586.
[23] Y. MITO AND T. J. HANRATTY, *Use of a modified Langevin equation to describe turbulent dispersion of fluid particles in a channel flow*, Flow Turb. Combustion, 68 (2002), pp. 1–26.
[24] ANSYS FLUENT V13.0, ANSYS Inc 2012, `http://www.ansys.com/`.
[25] T. HAYASE, J. A. C. HUMPHREY AND R. GRIEF, *A consistently formulated QUICK scheme for fast and stable convergence using finite-volume iterative calculation procedures*, J. Comput. Phys., 98 (1992), pp. 108–118.
[26] S. V. PATANKAR, Numerical Heat Transfer and Fluid Flow, Hemisphere, New York, 1980.